JPhys Energy

PAPER • OPEN ACCESS

Layered lithium niobium (III) oxide—$LiNbO_2$ as a visible-light-driven photocatalyst for H_2 evolution

JPhys Energy

PAPER

Layered lithium niobium (III) oxide—$LiNbO_2$ as a visible-light-driven photocatalyst for H_2 evolution

Xiaoxiang Xu[1,2], **Gang Liu**[3,4], **Shuang Ni**[5] **and John T S Irvine**[1]

[1] School of Chemistry, EaSTChem, University of St Andrews, St Andrews, Fife KY16 9ST, United Kingdom
[2] School of Chemical Science and Engineering, Tongji University, 1239 Siping Road, Shanghai 200092, People's Republic of China
[3] Shenyang National Laboratory for Materials Science, Institute of Metal Research, Chinese Academy of Science, 72 Wenhua RD, Shenyang 110016, People's Republic of China
[4] School of Materials Science and Engineering, University of Science and Technology of China, 72 Wenhua Road, Shenyang 110016, People's Republic of China
[5] Physical Chemistry Department, School of Chemistry and Materials Science, University of Science and Technology of China, Hefei, 230026, People's Republic of China

E-mail: jtsi@st-andrews.ac.uk

OPEN ACCESS

RECEIVED
8 June 2018

REVISED
17 July 2018

ACCEPTED FOR PUBLICATION
20 July 2018

PUBLISHED
20 November 2018

Keywords: photocatalysts, clean energy, layered semi conducting compound, hydrogen production

Supplementary material for this article is available online

Abstract

The search for visible-light photocatalysts is of great significance in clean energy and environmental applications to best utilize solar radiation. Some layered semiconductor photocatalysts have been found to exhibit promising performance levels. Their superior activity has been linked to the layering within the crystal structure, which may facilitate separation of carriers and, hence the reduction and oxidation reactions. Previous investigations on layered materials focused on oxides containing early transition metal cations with d^0 electronic configurations utilizing ultraviolet radiation. Attempts to synthesize layered materials with visible light response have been less successful and the photoactivity of such materials is not very high. Here, we have investigated a layered semiconducting compound, $LiNbO_2$ with nominal d^2 electronic configuration (Nb^{3+}). As a result of a sub-valence band originating from filled d orbitals, $LiNbO_2$ exhibits visible light absorption extending to 650 nm and demonstrates interesting photocatalytic activity for hydrogen production.

Solar energy is the most promising energy feedstock across the world due to its inexhaustible nature and environmental friendliness [1]. The distribution of solar incidence worldwide ensures easy accessibility of energy resource and wide applicability of solar technologies [2]. Among various solar technologies available, converting solar power directly into chemical fuels is one of most promising means of solar energy utilizations, as it can be readily adopted into our current energy infrastructure built upon fossil fuels [3, 4]. A typical example is solar hydrogen production from water [5, 6]. Under appropriate radiation conditions, preferably visible light, hydrogen is produced on the surface of a photocatalyst without any other energy input. Such a simple energy conversion process is very tempting, yet only a few materials were found be to photocatalytically active for hydrogen production without sacrificial elements, let alone an appreciable conversion efficiency under visible light radiation [7–10]. A number of layered compounds have been found to exhibit interesting photocatalytic activity [9, 11–25]. Their activity seems to be associated with the peculiar layered crystal structures that promote separation of charges and reactions [11, 13, 26, 27]. Previous investigations of layered compounds were largely limited to those active only under UV radiation [11, 13, 27–32]. Here, we investigated a layered compound $LiNbO_2$ with nominal d^2 electronic configuration that shows very high hydrogen production rate under visible light radiation.

The layered compound $LiNbO_2$ has been studied previously due to the occurrence of superconductivity at ~5 K if around 30% of the Li cations are removed [33, 34]. Its layered structure comprises of alternating NbO_6 trigonal prism sheets and layers of Li^+ cations (figure S1 is available in the supplementary material: stacks.iop.org/JPENERGY/1/015001/mmedia). Conductivity measurement and theoretical calculations suggest an

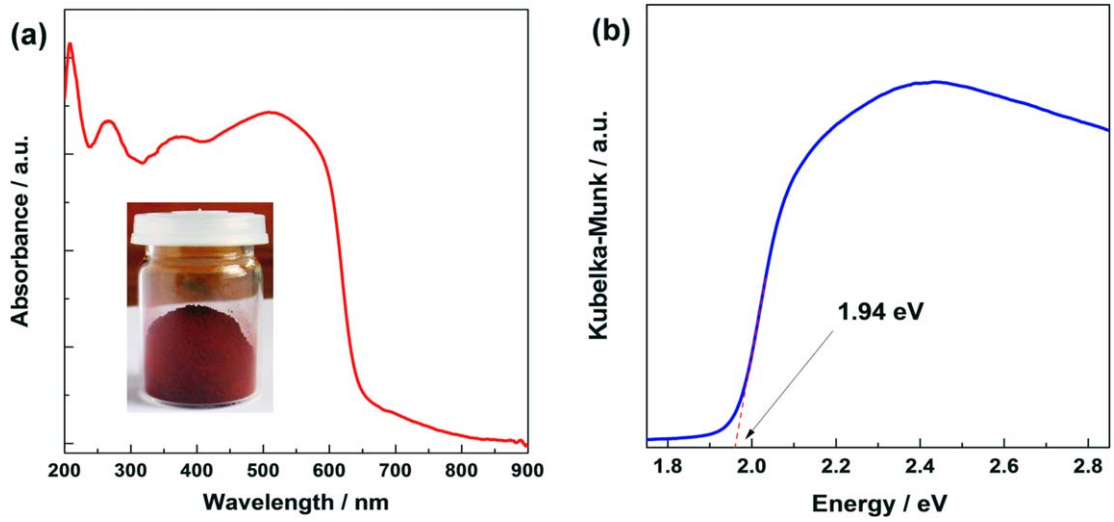

Figure 1. (a) UV-visible absorption spectrum of $LiNbO_2$ (converted from diffuse reflectance spectra) and photograph of $LiNbO_2$ powders are shown in the inserted images; (b) Kubelka–Munk transformation of reflectance data.

insulator-to-metal transition driven by decreasing Li content; zero or low deficiency of Li yields a semiconductor with band gap energy around 2 eV [34–37]. This bandgap indicates that semiconducting $LiNbO_2$ might be a promising photocatalyst despite the low oxidation state of Nb suggesting redox instability in contact with water. Recent results on cubic $Sr_{1-x}NbO_3$ demonstrate that reduced niobium oxides do not necessarily react with water at ambient conditions and hence can deliver stable photocatalytic activity in aqueous systems [7, 38], hence we have investigated layered $LiNbO_2$ as a possible photocatalyst.

Results and discussions

$LiNbO_2$ was synthesized by reacting Li_3NbO_4 and Nb_2O_5 precursors with Nb metal in a flowing Ar atmosphere [39]. The refined x-ray diffraction (XRD) patterns of the final sample obtained are displayed in figure 1S. All of the peaks can be indexed and refined in the hexagonal symmetry (space group $P6_3/mmc$) in accord with previous reports [33]. The final R factors ($R_{wp} = 8.57\%$ and $R_p = 6.69\%$) and the value of reduced χ^2 (2.015) suggest a reasonable fit of the structure model to the observed XRD patterns, confirmed by the absence of any unassigned peaks and, hence, no secondary phase in the sample. The refined unit cell parameters (a and c) and cell volume are (2.9100(3) Å and 10.4708(6) Å) and 76.78 (1) $Å^3$, respectively. Thermogravimetric analysis under flowing oxygen atmosphere suggests a weight gain of 12.08% up to 1000 °C, which agrees well with the theoretical value 12.13% on the assumption that all Nb cations in $LiNbO_2$ are oxidized to Nb^{5+} during the TGA in air. The molar ratio of Li to Nb is determined to be 0.95(7) based on inductively coupled plasma (ICP) measurements, which is very close to the stoichiometric value in ideal $LiNbO_2$.

In accord with previous reports and the reddish appearance of the powders, UV-visible absorption spectrum of the synthesized $LiNbO_2$, figure 1, reveals an intense absorption in the visible region with absorption extending as far as 650 nm. Kubelka–Munk transformation versus the energy of the light suggests an onset of light absorption starts from 1.94 eV (see inserted image in figure 1), which agrees well with a band gap ~2 eV and the reported semiconducting nature of the sample [37].

We evaluated the photocatalytic activity of $LiNbO_2$ for water splitting by monitoring H_2 production from oxalic acid aqueous solution under visible light irradiation. Oxalic acid is known as a common pollutant from industrial treatment processes such as textile industry and metallurgy, the low potential of its redox couple $H_2C_2O_4$ (aq)/CO_2 (g) = −0.49 V suggests that it can be used as a good hole scavenger [40]. Measurements were firstly carried out in the dark conditions with the purpose of evaluating any reaction that does not proceed photocatalytically. No H_2 was detected during the measured 5 h in the absence of radiation. Figure 2 displays the typical time courses of H_2 production under visible light radiation. Although only a trace of hydrogen was generated in the initial 2 h, the pristine $LiNbO_2$ (0.2 g) shows a hydrogen evolution rate of ca. 12 μmol h^{-1} in the subsequent experiment. The inducement period of the first two hours might be due to the passivated surface as samples were synthesized by annealing at ultra-high temperature (1250 °C) for 20 h. To acquire a sample with a large fresh surface, the as-prepared $LiNbO_2$ powders were then ball milled to break down the large particles (figure S2). The ball milled sample shows an apparent improvement on the hydrogen evolution rate

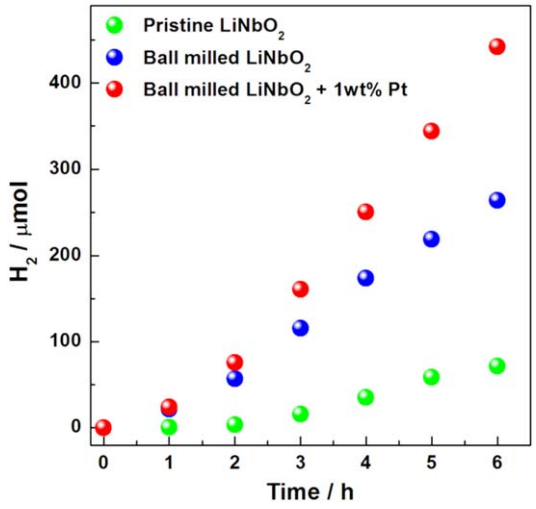

Figure 2. Time-dependent photocatalytic hydrogen evolution from pristine $LiNbO_2$, ball-milled $LiNbO_2$ and ball-milled $LiNbO_2$ with 1 wt% Pt. Measurements were performed upon 0.2 g powders in 200 ml oxalic acid aqueous solution (0.025 M). Light source: 250 W iron doped metal halide UV–vis lamp with a UV cut-off filter ($\lambda \geqslant 420$ nm).

(~44.2 μmol h^{-1}) by a factor of 3.6 with respect to the pristine one. Additionally, the inducement period is largely eliminated and a nearly linear hydrogen evolution rate is observed, suggesting good photocatalytic stability. The improved photocatalytic performance can be attributed to the large active surface created after ball milling as specific surface area increases from 1.2–9.1 m^2 g^{-1} as determined by BET analysis. Furthermore, the photocatalytic performance can be further improved by introducing Pt and an average H_2 production rate ~73.7 μmol h^{-1} was achieved by loading 1 wt% Pt, approaching an apparent quantum efficiency ca. 0.277%. The role of Pt in this experiment is as a co-catalyst that not only collects photo-generated charges but also provides additional reaction sites. Microscopic analysis indicates the formation of Pt nanoparticles (~10 nm) on the surface of $LiNbO_2$ with core-shelled micro-structures (figure S3). The action spectrum of photocatalytic hydrogen production showed a strong dependence upon the wavelength of photons with maximum performance around 600 nm (figure S4), confirming a real photocatalytic process. The corresponding apparent quantum efficiency reaches 1.8% at 550 nm. The linear sweep voltammogram based on $LiNbO_2$ thin film electrode clearly shows a light driven current response under chopped light (figure S5). Photocurrent was observed up to 650 nm and the plots of photocurrent versus wavelength roughly follow UV–vis absorption spectrum (figure S6). Other hole scavengers like methanol and sodium sulphite were also employed and steady hydrogen evolution was observed with apparent quantum efficiency ca. 0.38% under full range irradiation and without change in activity in repeated experiments (figure S7, table S1); the turnover number is calculated to be 7.18 according to the amount of hydrogen produced and number of atoms in the material [5]. Besides, the powders before and after photocatalytic experiment showed an identical XRD pattern (figure S8), SEM image (figure S9) and x-ray photoelectron spectroscopy (XPS) signals (figure S10). More interestingly, XPS spectra suggest the existence of Nb^{2+} and Nb^{4+} species, which implies $LiNbO_2$ is probably a charge transfer insulator and Nb only has an effective charge of 3+. Based on the above results, we confirm that $LiNbO_2$ is a real photocatalyst and is capable of splitting water in the presence of sacrificial elements. It should also be noted that the surface area of $LiNbO_2$ particles after ball-milling is still quite low and particles are fairly large (see figure S2) therefore the capability of photocatalytic hydrogen evolution may be improved by further decreasing the particle size. Mechanical processing will not only help to decrease the particle size but also may provide additional trapping sites that are favorable for reactions and charge separation.

To better understand the photocatalytic activity and its relation to the layered structure, we carried out some theoretical calculations on the electronic structure of $LiNbO_2$. The calculated band structure is displayed in figure 3. According to the calculations, conduction band and valence band are well separated from the Femi level with a direct band gap 1.6 eV, therefore, $LiNbO_2$ is indeed a semiconductor. The smaller calculated band gap compared to the experimental value (1.94 eV) is due to the drawbacks of GGA method that often underestimates band gap energy [41]. Nevertheless, the calculations do give useful qualitative information. Layered materials are well known for their anisotropies in physical or chemical properties, such as electronic conductivity of graphite. The question then arises whether the photogenerated charge carriers (electron hole pairs) behave in an anisotropic manner in the case of layered $LiNbO_2$. This can be examined by analyzing its band structure in different crystallographic directions (figure 3). Take for example, along *E–k* curve, traversing from point ***a*** to point ***b*** covers a large energy dispersion ~2 eV of conduction band in the [100] direction. Recalling that the

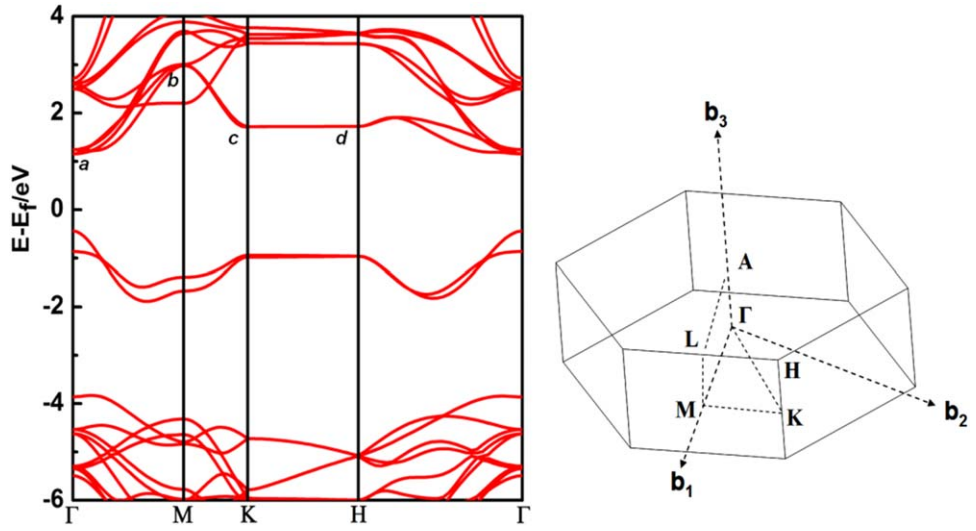

Figure 3. Calculated band structure of $LiNbO_2$, energy zero point was set at Fermi level. Brillouin zone for a hexagonal lattice was shown on the right.

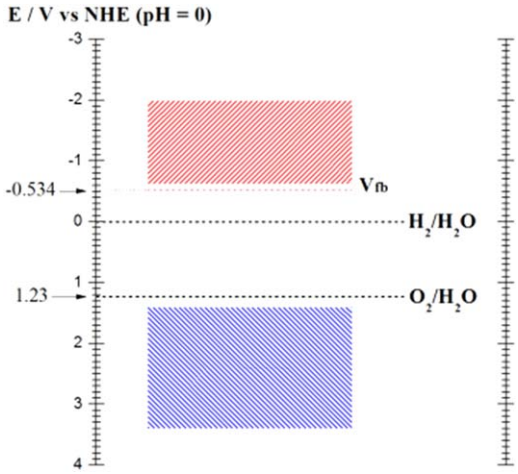

Figure 4. Proposed energy band positions for $LiNbO_2$ in comparison with redox potential of water at pH = 0.

mobility of electrons/holes is inversely proportional to their effective mass m^* and the effective mass is inversely proportional to the second derivative of E versus k curve (wide band leads to high mobility):

$$m^* = \hbar^2\left(\frac{d^2E}{dk^2}\right)^{-1} \quad (1)$$

therefore, the electrons in the CB will have a high mobility in the [100] direction [42, 43]. In other words, a large curvature of E–k curve indicates 'light' electrons/holes that are easy to move. Similar observations are also found in other directions such as [−120] (from point ***b*** to point ***c***), therefore, electrons are highly mobile parallel to the NbO_6 trigonal prism sheets. However, dispersion in the [001] direction (from point ***c*** to point ***d***) is almost negligible, suggesting electron migration across different layers are virtually forbidden. Similar situations are also found in the valence band thereby charge carriers in $LiNbO_2$ will be more or less restricted in separated layers. These restrictions to the charge carriers are of great significance to the photocatalytic activity, as electron hole recombination between different layers can be considerably mitigated.

Partial density of states (PDOS) from constituent elements in $LiNbO_2$ were also calculated (figure S11). The absence of Li PDOS near Fermi level suggests negligible contributions of Li to both CB and VB. The CB and VB are found to be predominantly composed by Nb atoms (4*d* orbitals), with some contributions from O atoms (mainly 2*p* orbitals). In this respect and above analysis, electrons and holes are primarily confined in the individual NbO_6 trigonal prism sheets with high intrasheet mobility. The role of interlayer Li^+ ions can therefore be understood as steric barriers preventing charge interactions between different sheets. This specific structure is

highly beneficial for fast charge transfers as each NbO_6 trigonal prism sheet can act as an independent photocatalyst.

Knowledge of the energy band positions is also crucial in understanding the photocatalytic reactions. The conduction band edge can be roughly inferred from the Mott–Schottky (MS) plot according to impedance measurement (figure S12). The flat-band potential determined from MS plot ~−0.534 V versus NHE will lie very close to the conduction band edge. Thereby the valence band edge can be simply estimated using the band gap energy (1.94 eV), which approximately lies at +1.4 V versus NHE. The final proposed energy band positions are displayed in figure 4. The energy gap between CB and VB straddles the redox potentials of water, which meets the thermodynamic requirement for water splitting. Nevertheless, the CB edge is suitably more negative (<−0.534 V versus NHE) than the reduction potential of water, so the electrons in the conduction band will have high reducing power for hydrogen evolution and a strong driving force for the separation from holes due to the large potential drop across depletion layer when equilibrating with water. The VB edge, on the other hand, lies very close to the oxidation potential of water, suggesting $LiNbO_2$ might not be suitable for O_2 production. This is confirmed in the photocatalytic O_2 evolution experiment (table S2), where only a small amount of O_2 was produced even under full range radiation (UV + Vis) and a low turnover number around 0.07.

Conclusions

In summary, we have synthesized a layered compound $LiNbO_2$, which demonstrates a high photocatalytic activity in H_2 production. Its good photocatalytic performance might be related to the anisotropic dispersion of its electronic structure such that charge recombination can be inhibited. The very negative CB edge position endows photogenerated electrons with high reducing power and facile charge separation that favors H_2 production. Such a layered structure as well as the special d^2 electronic configurations of transition metal enlightens our search for new photoactive materials in the future.

Methods

Sample synthesis

$LiNbO_2$ was synthesized by calcining homogenized Li_3NbO_4, Nb and Nb_2O_5 mixtures in a flowing Ar atmosphere at 1250 °C for 20 h [33, 39]. Details for synthesis can be found in supplementary information.

Characterization

Crystal structure and phase purity were examined by XRD analysis of powders on a STOE STADI/P powder diffractometer. Incident radiation was generated using a CuKα1 source (λ = 1.540 56 Å). The step size for data collection was 0.02° with a collection time 1000 s at each step. Vaseline was used to mount the powders onto the holder. X-POW software and General Structure Analysis System program under EXPGUI interface was used to perform least square refinement and Rietveld refinement. A Micromeritics instrument ASAP 2020 was used to examine the N_2 adsorption and desorption properties and specific surface areas were calculated via the Brunauer–Emmett–Teller (BET) model. The microstructure of the powders was inspected using a scanning electron microscope (JEOL 5600 SEM) equipped with a Mica energy dispersive x-ray spectroscopy analysis system. Diffuse reflectance spectra were collected on a UV–vis spectrophotometer (JASCO-V550) and the absorbance was transformed by the Kubelka–Munk method. Thermogravimetric analysis was carried out on a Rheometric Scientific TG 1000M+ and TA instruments with heating and cooling rate of 10 °C min^{-1} to 1000 °C under flowing oxygen. An Agilent 7500a ICP mass spectroscopy with laser ablation was used for surface element analysis. MS analysis was carried out through impedance measurements using a Schlumberger Solartron 1255 frequency response analyzer couple with a 1287 Electrochemical Interface. Sintered $LiNbO_2$ pellet, Pt wire, Ag/AgCl electrode and 1 M KCl aqueous solution were used as working, counter, reference electrode and electrolyte respectively. The configuration of the set up was as decribed in prior literature [44]. The impedance analysis was performed at frequency range from 100 kHz–0.1 Hz at 50 mV rms under potential bias from −1.6 to +0.5 V (versus Ag/AgCl). The capacitance was then extracted from the impedance spectra and was used to derive the MS plot. The XPS measurements were performed on Thermo Escalab 250 with a monochromatic Al K_α x-ray source. All binding energies were referenced to the C 1 s peak (284.6 eV) arising from adventitious carbon.

Photoreactivity measurements

Measurement of photocatalytic hydrogen evolution was performed in a home-made Teflon reactor with window sealed by a quartz glass. In a typical experiment, photocatalyst was dispersed in aqueous solution (oxalic acid, Methanol or sodium sulfite). The suspension was then sealed within the home-made photoreactor. The

reactor was purged with pure Ar gas as a protective gas. Gas composition within the reactor was monitored by a gas chromatograph (Agilent 3000 Micro Gas Chromatograph). A 250 W iron doped metal halide UV–vis lamp with or without a UV cut-off filter ($\lambda \geqslant 420$ nm) was used as the light source. The photon flux of the lamp is calibrated using a quantum meter (Apogee MQ-200). The average photon flux is 1305 $\pm$ 27 μmol m^{-2} s^{-1} under visible light radiation and 1510 $\pm$ 31 μmol m^{-2} s^{-1} under full range radiation. The photocatalytic oxygen evolution was performed in a similar set up, except using 0.1 g $LiNbO_2$ powder and 200 ml $AgNO_3$ aqueous solution (0.005 M) as a sacrificial element.

The $LiNbO_2$ thin film electrode was prepared according to the following procedure: 40 mg powders and 10 mg iodine were dispersed in 50 ml acetone solution ultrasonically. Two pieces of fluorine-doped tin oxide (FTO) glasses were then placed in parallel into the suspension with a separate distance 10 mm. 30 V bias was applied for 30 min between these two FTO glass under potentiostatic control. The as-prepared electrode was then dried in the oven for 1 h before photocurrent measurements. The photocurrent measurements were performed in 0.2 M Na_2SO_4 aqueous solution using $LiNbO_2$ thin film electrode, platinum sheet and Ag/AgCl electrode as working, counter and reference electrode respectively.

Theoretical calculations

Theoretical calculations were carried out by using the density functional theory implemented in the Vienna *ab initio* simulation package [45]. Perdew, Burke and Ernzerhof exchange-correlation functional within the generalized gradient approximation [46] and the projector augmented-wave pseudopotential [47] were adopted. Spin-polarization was also taken into account in this calculation. A hexagonal super cell with $a = 2.91$ Å and $c = 10.47$ Å was used for simulations. All geometry structures were fully relaxed until the forces on each atom are less than 0.01 eV $Å^{-1}$. Static calculations were done with a 19 $\times$ 19 $\times$ 5 Monkhorst–Pack k-point grid [48].

Acknowledgments

The authors thank the Engineering and Physical Sciences Research Council (EPSRC EP/K006800/1, EP/K022237/1) and Anglo American Platinum for financial support and the Royal Society for a Wolfson Merit Award. Origina data can be found on the University of St Andrews' research portal (https://doi.org/10.17630/00c8efe5-df65-4561-9711-69f165b75549).

Author contributions

XX performed the synthesis and collected data with GL and SN carried out the theoretical calculations. All the authors contributed to the writing of the manuscript.

Additional information

The authors declare no competing financial interests[6].

ORCID iDs

John T S Irvine https://orcid.org/0000-0002-8394-3359

Referencecs

[1] Lewis N S and Nocera D G 2006 Powering the planet: chemical challenges in solar energy utilization *Proc. Natl Acad. Sci. USA* **103** 15729–35
[2] Osterloh F E 2008 Inorganic materials as catalysts for photochemical splitting of water *Chem. Mater.* **20** 35–54
[3] Hoffmann M R, Martin S T, Choi W Y and Bahnemann D W 1995 Environmental Applications of semiconductor photocatalysis *Chem. Rev.* **95** 69–96
[4] Listorti A, Durrant J and Barber J 2009 Artificial photosynthesis solar to fuel *Nat. Mater.* **8** 929–30
[5] Kudo A and Miseki Y 2009 Heterogeneous photocatalyst materials for water splitting *Chem. Soc. Rev.* **38** 253–78
[6] Chen X B, Shen S H, Guo L J and Mao S S 2010 Semiconductor-based photocatalytic hydrogen generation *Chem. Rev.* **110** 6503–70
[7] Xu X X, Randorn C, Efstathiou P and Irvine J T S 2012 A red metallic oxide photocatalyst *Nat. Mater.* **11** 595–8
[8] Zou Z G, Ye J H, Sayama K and Arakawa H 2001 Direct splitting of water under visible light irradiation with an oxide semiconductor photocatalyst *Nature* **414** 625–7

[6] The research data supporting this publication can be accessed at: https://doi.org/10.17630/00c8efe5-df65-4561-9711-69f165b75549 (reference 49).

[9] Wang X C *et al* 2009 A metal-free polymeric photocatalyst for hydrogen production from water under visible light *Nat. Mater.* **8** 76–80
[10] Maeda K *et al* 2006 Photocatalyst releasing hydrogen from water-enhancing catalytic performance holds promise for hydrogen production by water splitting in sunlight *Nature* **440** 295
[11] Miseki Y, Kato H and Kudo A 2009 Water splitting into H-2 and O-2 over niobate and titanate photocatalysts with (111) plane-type layered perovskite structure *Energ. Environ. Sci.* **2** 306–14
[12] Takata T *et al* 1997 Photocatalytic decomposition of water on spontaneously hydrated layered perovskites *Chem. Mater.* **9** 1063
[13] Kudo A, Kato H and Nakagawa S 2000 Water splitting into H-2 and O-2 on new $Sr_2M_2O_7$ (M = Nb and Ta) photocatalysts with layered perovskite structures: factors affecting the photocatalytic activity *J. Phys. Chem.* B **104** 571–5
[14] Takata T, Tanaka A, Hara M, Kondo J N and Domen K 1998 Recent progress of photocatalysts for overall water splitting *Catal. Today* **44** 17–26
[15] Kako T, Zou Z and Ye J 2005 Photocatalytic oxidation of 2-propanol in the gas phase over cesium bismuth niobates under visible light irradiation *Res. Chem. Intermediat.* **31** 359–64
[16] Li Y X, Chen G, Zhang H J, Li Z H and Sun J X 2008 Electronic structure and photocatalytic properties of ABi(2)Ta(2)O(9) (A = Ca, Sr, Ba) *J. Solid State Chem.* **181** 2653–9
[17] Liu G *et al* 2010 Unique electronic structure induced high photoreactivity of sulfur-doped graphitic C_3N_4 *J. Am. Chem. Soc.* **132** 11642–8
[18] Sun X Q *et al* 2015 Photocatalytic hydrogen production over chromium doped layered perovskite Sr_2TiO_4 *Inorg. Chem.* **54** 7445–53
[19] Lv M L, Liu G and Xu X X 2016 Homologous compounds $Zn_nIn_2O_{3+n}$ (n = 4, 5 and 7) containing laminated functional groups as efficient photocatalyt for hydrogen production *ACS Appl. Mater. Interfaces* **8** 28700–8
[20] Chen H M, Sun X Q and Xu X X 2017 Ruddlesden–Popper compounds (SrO)($LaFeO_3$)n (n = 1 and 2) as p-type semiconductors for photocatalytic hydrogen production *Electrochim. Acta* **252** 138–46
[21] Chen H M and Xu X X 2017 Ruddlesden–Popper compounds in the double-perovskite family Sr_2FeTaO_6(SrO) (n = 0, 1 and 2) and their photocatalytic properties *Appl. Catal.* B **206** 35–43
[22] Lv M L *et al* 2017 Ultrathin lanthanum tantalate perovskite nanosheets modified by nitrogen doping for efficient photocatalytic water splitting *ACS Nano* **11** 11441–8
[23] Sun X Q and Xu X X 2017 Efficient photocatalytic hydrogen production over La/Rh co-doped Ruddlesden–Popper compound Sr_2TiO_4 *Appl. Catal.* B **210** 149–59
[24] Sun X Q, Mi Y L, Jiao F and Xu X X 2018 Activating layered perovskite compound Sr_2TiO_4 via La/N codoping for visible light photocatalytic water splitting *ACS Catal.* **8** 3209–21
[25] Wei S H and Xu X X 2018 Boosting photocatalytic water oxidation reactions over strontium tantalum oxynitride by structural laminations *Appl. Catal.* B **228** 10–8
[26] Liu G, Wang L Z, Yang H G, Cheng H M and Lu G Q 2010 Titania-based photocatalysts-crystal growth, doping and heterostructuring *J. Mater. Chem.* **20** 831–43
[27] Sayama K *et al* 1998 Photocatalytic activity and reaction mechanism of Pt-intercalated $K_4Nb_6O_{17}$ catalyst on the water splitting in carbonate salt aqueous solution *J. Photochem. Photobiol.* A **114** 125–35
[28] Ikeda S *et al* 1998 Preparation of $K_2La_2Ti_3O_{10}$ by polymerized complex method and photocatalytic decomposition of water *Chem. Mater.* **10** 72–7
[29] Ikeda S *et al* 1998 Preparation of a high active photocatalyst, $K_2La_2Ti_3O_{10}$, by polymerized complex method and its photocatalytic activity of water splitting *J. Mater. Res.* **13** 852–5
[30] Machida M, Yabunaka J and Kijima T 2000 Synthesis and photocatalytic property of layered perovskite tantalates, RbLnTa(2)O(7) (Ln = La, Pr, Nd, and Sm) *Chem. Mater.* **12** 812–7
[31] Miseki Y, Kato H and Kudo A 2005 Water splitting into H-2 and O-2 over $Cs_2Nb_4O_{11}$ photocatalyst *Chem. Lett.* **34** 54–5
[32] Li Y X, Chen G, Zhang H J and Lv Z S 2010 Band structure and photocatalytic activities for H-2 production of ABi(2)Nb(2)O(9) (A = Ca, Sr, Ba) *Int. J. Hydrog. Energy* **35** 2652–6
[33] Geselbracht M J, Richardson T J and Stacy A M 1990 Superconductivity in the layered compound Li_xNbO_2 *Nature* **345** 324–6
[34] Turzhevsky S A, Novikov D L, Gubanov V A and Freeman A J 1994 Electronic-structure and crystal-chemistry of niobium oxide phases *Phys. Rev.* B **50** 3200–8
[35] Novikov D L, Gubanov V A, Zubkov V G and Freeman A J 1994 Electronic-structure and electron–phonon interactions in layered Li_xNbO_2 and Na_xNbO_2 *Phys. Rev.* B **49** 15830–5
[36] Ylvisaker E R and Pickett W E 2006 First-principles study of the electronic and vibrational properties of $LiNbO_2$ *Phys. Rev.* B **74** 075104
[37] Geselbracht M J, Stacy A M, Garcia A R, Silbernagel B G and Kwei G H 1993 Local environment and lithium ion mobility in $LiNbO_2$—inferences from structure, physical-properties, and NMR *J. Phys. Chem.* **97** 7102–7
[38] Efstathiou P, Xu X X, Menard H and Irvine J T S 2013 An investigation of crystal structure, surface area and surface chemistry of strontium niobate and their influence on photocatalytic performance *Dalton Trans.* **42** 7880–7
[39] Peng N H, Irvine J T S and Fitzgerald A G 1998 Synthesis and crystal structure of the distorted perovskite $Sr_{0.97}NbO_3$ determined by high resolution powder neutron diffraction *J. Mater. Chem.* **8** 1033–8
[40] Herrmann J M, Mozzanega M N and Pichat P 1983 Oxidation of oxalic-acid in aqueous suspensions of semiconductors illuminated with UV or visible-light *J. Photochem.* **22** 333–43
[41] Xiao H, Tahir-Kheli J and Goddard W A 2011 Accurate band gaps for semiconductors from density functional theory *J. Phys. Chem. Lett.* **2** 212–7
[42] Kittel C 1996 *Introduction to Solid State Physics* 7th edn (New York: Wiley)
[43] Mizoguchi H and Woodward P M 2004 Electronic structure studies of main group oxides possessing edge-sharing octahedra: implications for the design of transparent conducting oxides *Chem. Mater.* **16** 5233–48
[44] Gelderman K, Lee L and Donne S W 2007 Flat-band potential of a semiconductor: using the Mott–Schottky equation *J. Chem. Educ.* **84** 685–8
[45] Kresse G and Furthmuller J 1996 Efficient iterative schemes for *ab initio* total-energy calculations using a plane-wave basis set *Phys. Rev.* B **54** 11169–86
[46] Perdew J P, Burke K and Ernzerhof M 1996 Generalized gradient approximation made simple *Phys. Rev. Lett.* **77** 3865–8
[47] Kresse G and Joubert D 1999 From ultrasoft pseudopotentials to the projector augmented-wave method *Phys. Rev.* B **59** 1758–75
[48] Monkhorst H J and Pack J D 1976 Special points for Brillouin-zone integrations *Phys. Rev.* B **13** 5188–92